IEEE Access
Multidisciplinary | Rapid Review | Open Access Journal

Received July 21, 2020, accepted August 8, 2020, date of publication September 10, 2020, date of current version September 24, 2020.

Digital Object Identifier 10.1109/ACCESS.2020.3023248

User Influence on Polarization Characteristics in Off-Body Channels

KENAN TURBIC[1], (Member, IEEE), MARIELLA SÄRESTÖNIEMI[2], (Member, IEEE), MATTI HÄMÄLÄINEN[2], (Senior Member, IEEE), AND LUIS M. CORREIA[1], (Senior Member, IEEE)

[1]INESC-ID/IST, University of Lisbon, 1000-029 Lisbon, Portugal
[2]Centre for Wireless Communications (CWC), University of Oulu, 90014 Oulu, Finland

Corresponding author: Kenan Turbic (kenan.turbic@tecnico.ulisboa.pt)

This work was supported in part by the Academy of Finland 6Genesis Flagship (Grant 318927), WBAN Communications in the Congested Environments (MeCCE) Project and the European Union's Horizon2020 Programme under the Marie Sklodowska-Curie Grant agreement No. 872752.

ABSTRACT This article investigates the impact of the user's body on wearable antenna radiation characteristics and the consequent effects on the off-body channel, with the focus on the polarization aspect. The impact on antenna gain and polarization is analyzed for different antenna placements and separations from the body, based on electromagnetic simulations with numerical phantoms at 3, 4 and 5 GHz. Results show a strong influence of the body on the antenna efficiency, gain, and polarization. The excess losses due to body-shadowing suppress the antenna radiation behind the body by more than 20 dB, while its polarization changes from vertical in free space, to an elliptical one when placed on the body. The obtained radiation characteristics are then employed for off-body channel simulations using a geometry-based polarized channel model, which employs an analytic mobility model for wearable antennas based on Fourier series. The antenna rotation due to changes in user's posture is seen as one of the main sources of off-body channel degradation. The polarization mismatch losses imposed by antennas' physical misalignment, are observed to yield periodic fades of the Line-of-Sight component, with more than 30 dB drops in the received power level.

INDEX TERMS Body area networks, body shadowing, depolarization, dynamic users, off-body channel, wearable antennas, ultra-wideband (UWB).

I. INTRODUCTION

The employment of remote monitoring systems is recently being considered in various domains, with applications in healthcare, military, sports and entertainment, among others, showing potential to provide revolutionary solutions for the existing problems. Healthcare is one of the most attractive application domains, where the employment of these systems is greatly motivated by the aging demographics of the global population [1].

At the front end of these systems, Body Area Networks (BANs) consisting of a number of inter-connected sensor devices operating on and inside of the body can be used to measure users' versatile psycho-physiological and environmental parameters [2], [3], and transfer this information to remote data centers by exploiting the off-body communication infrastructure. BAN devices need to be not only small, light-weight and comfortable to wear, but also safe and energy-efficient to enable a lifetime of several months or even years. While essential for BANs' widespread adoption, these requirements impose great challenges on system design.

A number of standardized radio technologies can be employed for communications within BANs and with off-body devices, including Bluetooth Low Energy (BLE) [4] and the IEEE802.11-family [5], but also dedicated standards IEEE802.15.6 [6] and ETSI SmartBAN [7]. While some frequencies are dedicated for sensitive medical applications, e.g. MBAN band at 2.36 - 2.40 GHz, most of these technologies operate in the unlicensed Industrial, Scientific and Medical (ISM) band starting from 2.4 GHz, where interference and co-existence issues pose a challenge. The Ultra-wideband (UWB) technology [6] provides means to combat these issues with its inherently low power spectral density, due to the low

The associate editor coordinating the review of this manuscript and approving it for publication was Faisal Tariq.

transmission power and extremely large signal bandwidth, i.e. exceeding 500 MHz. High available data rates, immunity to interference and low radiation exposure of users make UWB a popular choice for BANs.

Regardless of the radio technology, wearable antennas are an essential part of BAN devices and their ability to efficiently radiate and capture energy has a major impact on communication quality and overall system performance. As these antennas operate in the proximity of lossy body tissues, their performance is greatly affected by the user. Based on measurements [8]–[10] and Electromagnetic (EM) simulations [11]–[13], the antenna efficiency is reported to be strongly impacted by the body for separations below 8 mm, while this impact is negligible when the antenna is more than 15 mm away from the body. Moreover, different body types [10], [14] and on-body antenna locations [15]–[19] have a clear impact on the radiation characteristics. In addition to the de-tuning effect as the resonant frequency is shifted [8], [19]–[21], the antenna bandwidth also changes in the proximity of the body [8], [19]–[23].

The body influence on the antenna gain pattern is reported in [14], [19], [20], [24], [25], where body-shadowing is observed as the dominant effect, yielding suppressed antenna radiation in the back direction. However, a slight gain improvement in the directions away from the body was also reported [9], [19]. These effects have recently attracted attention in mobile communications at the millimeter-wave band, where studies report a strong distortion of the radiation pattern and reduced coverage efficiency in the body proximity [26]–[28].

Antenna polarization and its impact on body area propagation has been studied, e.g., in [2], [8], [29], [30]. The influence of the body on wearable antenna polarization is the least explored aspect, with only a few preliminary studies available in literature [15], [31], [32]. With antennas operating on the body, the off-body transmission coefficients in channels established with vertical (V)- and horizontal (H)-polarized off-body antennas are observed to change compared to the free space case, due to polarization mismatch losses [8]. The radiated signal polarization was reported to change from a linear one in free space, to an elliptical one with the antenna on the body [31], [32]. However, a dedicated study of the body influence on antennas' polarization characteristics has not been previously reported.

Wearable antenna impairments in the body proximity have consequent impact on BAN communication channels, while the user's motion also has an important influence. Most of the available BAN channel studies are based on measurements and report empirical models, where the mean path loss is modeled by a distance power law, while large- and small-scales fading are represented via random variables. The most common statistical models for the two fading components are the Lognormal and Nakagami Distributions, respectively, while composite fading distributions derived from the κ-μ one are reported to provide a superior fit for shadowed channels [33].

However, these models typically fail to capture the effects associated with signal depolarization and user dynamics. These two effects are addressed only in a few measurement-based studies [34], [35], but some modeling efforts were also reported recently. A geometry-based stochastic on-body channel model is presented in [36], taking the depolarization due to path geometry into account. The model is expanded in [37], by additionally considering the material-dependent depolarization upon scattering. However, this model assumes static antennas and the impact of motion is reduced to the Doppler effect due to the forward movement at constant velocity. While this assumption is justified for on-body locations invariant to posture, e.g. on the head, it misrepresents the motion of antennas on arms and legs.

This was observed in [38], where a geometry-based polarized off-body channel model for BANs with dynamic users is proposed. The channel model was used to investigate different signal depolarization mechanisms, and the on-body antenna rotation during a motion cycle is found to be the main source of polarization mismatch losses. This observation was exploited to simplify the channel model in [39].

In summary, the user's body and motion have a significant impact on wearable antennas' performance and BAN communication channels. However, the polarization aspect of these effects has been mostly neglected in literature, while the few available studies show significant antenna depolarization in proximity of the body and a major impact of user dynamics on the polarization mismatch losses, especially due to the antenna rotation. Moreover, the off-body channel model presented in [38] seems to be the only model in the literature to jointly represent the depolarization effect and the influence of user dynamics.

This article investigates different aspects of user's influence on off-body BAN channels, with a focus on the polarization aspect. By considering a wearable UWB antenna, the impact of the body on the impedance matching, gain, and polarization characteristics is first investigated via numerical EM simulations. The consequent effects on the off-body channel are then analyzed based on simulations employing a channel model for polarized off-body communications with dynamic users. The main contribution of this article is in the analysis of the body influence on polarization characteristics, and the joint consideration of signal depolarization and of user's motion influence. To the best of the authors' knowledge, such a comprehensive study addressing these aspects of off-body BAN communications has not been previously reported. This article is a significant extension and expansion to previous work reported in [40].

The rest of the paper is structured as follows. Section II presents the models and metrics considered in this work, followed by the analysis of the effects of body proximity on wearable antenna's efficiency, gain and polarization characteristics in Sections III, IV and V, respectively. The consequent effects on the off-body channel are investigated in Section VI. The paper is concluded in Section VII.

II. MODELS AND METRICS

This section presents the metrics, and antenna and channel models considered in this work. The reference coordinate system associated with the antenna is introduced first, followed by the definitions of the planar and spherical metrics used to evaluate the impact the user's body on the radiation characteristics. The UWB antenna design is then described, and the channel model used to evaluate the impact on the off-body communication is presented.

A. COORDINATE SYSTEM AND METRICS

1) ANTENNA COORDINATE SYSTEM

The coordinate system associated with the wearable antenna is shown in Fig. 1. The antenna plane is assumed to lie within the yz-plane, with the x-axis pointing in the direction away from the body. With the given coordinate system reference, the antenna gain is obtained for uniformly sampled azimuth and elevation angles, with a 1° step. The gain patterns are obtained in θ- and ϕ- polarizations, with the corresponding reference vectors $\mathbf{u}_\theta$ and $\mathbf{u}_\phi$, respectively, being illustrated in Fig. 1 for an arbitrary Direction of Departure (DoD).

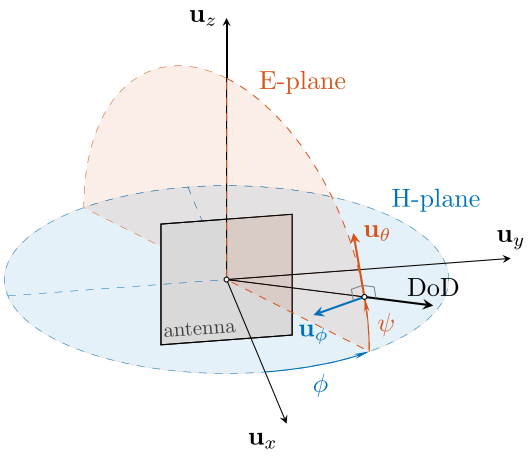

FIGURE 1. Antenna coordinate system.

For the vertical antenna orientation shown in the figure, the θ- and ϕ-components correspond to the V- and H-polarizations, respectively, therefore, the latter reference is used to refer to the two orthogonal polarization components in the rest of this article. However, it is important to point out that a wearable antenna on a dynamic user exhibits rotation due to the changing posture, hence, the θ/ϕ polarization reference rotates over time and generally does not align with the V/H one.

2) INPUT REFLECTION, GAIN AND CROSS-POLARIZATION ISOLATION

The evaluation of the antenna radiation characteristics are based on the input reflection coefficient, S_{11}, absolute realized gain, G, and Cross-Polarization Isolation (XPI), X_{pi}. While the first parameter describes the radiation efficiency, the other two characterize the spatial selectivity and polarization properties of the radiated signals. The absolute gain is calculated from the field gains obtained in the orthogonal polarizations, according to:

$$G(\phi,\psi)_{[\mathrm{dBi}]} = 20\log\left(\sqrt{|g_\phi(\phi,\psi)|^2+|g_\theta(\phi,\psi)|^2}\right) \quad (1)$$

where:

- ϕ Azimuth Angle of Departure (AAoD);
- ψ Elevation Angle of Departure (EAoD);
- $g_{\theta/\phi}$ field gain in θ/ϕ-polarization.

It is important to note that the antenna gain presented in this article refers to the realized one [41], which takes the losses due to input impedance mismatch into account, hence, the input reflection coefficient values at the considered frequencies being embedded.

The antenna XPI is obtained as the ratio of the transmitted signal power in the orthogonal polarizations, i.e.

$$X_{pi}(\phi,\psi)_{[\mathrm{dB}]} = 20\log\left|\frac{g_\theta(\phi,\psi)}{g_\phi(\phi,\psi)}\right| \quad (2)$$

In order to evaluate the impact of the user's body on radiation characteristics, the input reflection coefficient, gain and XPI obtained in the proximity of the body are compared to the values obtained in free space. As a quantitative measure, the corresponding relative metrics are calculated as follows:

$$\Delta S_{11\,[\mathrm{dB}]}(f) = S_{11}^{b}(f)_{[\mathrm{dB}]} - S_{11}^{fs}(f)_{[\mathrm{dB}]} \quad (3)$$

$$\Delta G(\phi,\psi)_{[\mathrm{dB}]} = G^{b}(\phi,\psi)_{[\mathrm{dBi}]} - G^{fs}(\phi,\psi)_{[\mathrm{dBi}]} \quad (4)$$

$$\Delta X_{pi}(\phi,\psi)_{[\mathrm{dB}]} = X_{pi}^{b}(\phi,\psi)_{[\mathrm{dB}]} - X_{pi}^{fs}(\phi,\psi)_{[\mathrm{dB}]} \quad (5)$$

where:

- f frequency.

The superscripts b and fs in (3)-(5) denote the values corresponding to the cases with the antenna on the body and in free space, respectively.

3) SPHERICAL STATISTICS

For a global quantification of the body influence on the antenna radiation, i.e. by considering all directions, spherical statistics evaluated over an imaginary radiation sphere enclosing the antenna are considered. This sphere is assumed to be in the far field zone, and points on its surface can be associated with the antenna gain and polarization in the corresponding direction; therefore, the spatial distributions of antenna gain and XPI can be expressed in terms of their distributions over the radiation sphere.

A spherical Cumulative Distribution Function (CDF) of the antenna gain is calculated as the ratio between the spherical area over which the gain is below a given threshold value and the total area of the sphere. With the uniform sampling in azimuth and elevation angles, the spherical CDF of the

antenna gain is calculated according to:

$$P\Big\{G(\phi,\psi) \le G_{th}\Big\} = \frac{\Delta\phi\,\Delta\psi}{4\pi}\sum_{k=1}^{N_\phi}\sum_{n=1}^{N_\psi}\mathbb{I}(G(\phi_k,\psi_n) \le G_{th})\cos\psi_n \quad (6)$$

where:

- N_ϕ number of azimuth angle samples, i.e. 361;
- N_ψ number of elevation angle samples, i.e. 181;
- $\Delta\phi$ azimuth angle uniform sampling step, i.e. $\pi/180$;
- $\Delta\psi$ elevation angle uniform sampling step, i.e. $\pi/180$;
- $\mathbb{I}(.)$ indicator function, i.e. 1 if the condition in the argument is satisfied and 0 otherwise.

This definition is similar to the one of spherical coverage or coverage efficiency, being recently used to evaluate mobile terminal performance and user blockage effects in millimeter-wave communications [26], [27], [42]. The cosine term in (6) follows from the determinant of the Jacobian matrix of the transformation from Cartesian to polar coordinates [43], and accounts for the fact that a uniform elevation angle sampling yields a higher density of samples towards the poles. It is important to note that the area ratio defining the spherical CDF is independent of the sphere's radius.

To distinguish between the spatial directions in which the antenna radiation improves or deteriorates in the body-proximity, the radiation sphere is divided into two regions, corresponding to the directions where the gain is higher/lower than in free space, i.e.

$$\mathcal{R}_+(\Delta G): \Big\{(\phi,\psi) \mid \Delta G(\phi,\psi)_{[\mathrm{dB}]} \ge 0\Big\} \quad (7)$$

$$\mathcal{R}_-(\Delta G): \Big\{(\phi,\psi) \mid \Delta G(\phi,\psi)_{[\mathrm{dB}]} < 0\Big\} \quad (8)$$

The average gain within these regions is calculated as a weighted sum of gain samples, with the fractions of the total sphere corresponding to spherical patches associated with each gain/XPI sample acting as weighting factors, i.e.

$$\overline{G(\phi,\psi)}_{[\mathrm{dBi}]}|\mathcal{R}_\pm = \frac{\sum_{\mathcal{R}_\pm} G(\phi_k,\psi_n)_{[\mathrm{dBi}]}\cos\psi_n}{\sum_{\mathcal{R}_\pm}\cos\psi_n} \quad (9)$$

where $\mathcal{R}_\pm$ in the subscript of the sum denotes summation over directions (ϕ_k,ψ_n) within that region. The corresponding standard deviation is similarly obtained, i.e.

$$\sigma\Big\{G(\phi,\psi)\Big\}_{[\mathrm{dB}]}|\mathcal{R}_\pm = \sqrt{\frac{\sum_{\mathcal{R}_\pm}\left[G(\phi_k,\psi_n)_{[\mathrm{dBi}]} - \overline{G(\phi_k,\psi_n)}_{[\mathrm{dBi}]}\right]^2\cos\psi_n}{\sum_{\mathcal{R}_\pm}\cos\psi_n}} \quad (10)$$

One should note that only the expressions for the antenna gain are provided herein, while the same definitions and expressions hold for the XPI, i.e., the spherical CDF, mean and standard deviation are calculated from (6)-(10), with G and ΔG replaced with X_{pi} and ΔX_{pi}, respectively.

B. WEARABLE UWB LOOP ANTENNA

This article considers a UWB loop antenna, previously presented in [44]. The antenna has an operational bandwidth within [3.1, 10.6] GHz in free-space, and has been designed for on- and off-body communications, compliant with the BAN standard [6]. The substrate of the originally presented antenna [44] was FR-4 [45], but it was later changed to Taconic TRF-43 [46] due to its better performance, especially in terms of the loss tangent [11]. The radiation characteristics of the antenna with the TRF-43 substrate are presented more in detail in [11], [12]. It should be pointed out that this antenna was previously used in several BAN channel measurement campaigns [47], [48].

The radiation characteristics of the antenna are considered at 3, 4 and 5 GHz, as these frequencies outline the UWB low-band [6], representing its lowest, center and highest frequencies, respectively. Fig. 2 shows the antenna gain and XPI in free space at the center frequency, i.e. 4 GHz. The antenna gain pattern has a slightly elongated doughnut shape, i.e. similar to a dipole, with the higher gain in azimuth directions at 0° and 180°. The extent of energy focusing in these directions is seen to increase with frequency, with the Half-Power Beam-Widths (HPBWs) in the azimuth and elevation plane decreasing from 83° to 71° and from 97° to 75°, respectively, as the frequency changes from 3 to 5 GHz. The antenna is dominantly V-polarized, as indicated by the red tones in the XPI plot (Fig. 2b), with almost ideal V-polarization observed at 0° and 180° azimuth directions, where the gain is maximal. XPI is around 20 dB in most directions, except for the area near poles, where radiation nulls are located.

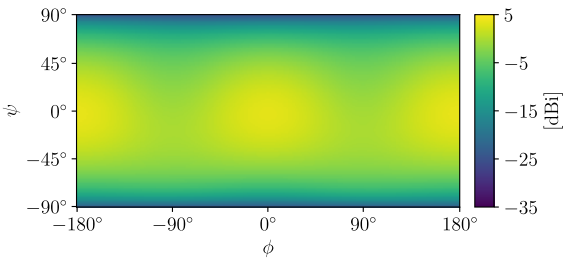

(a) Realized gain.

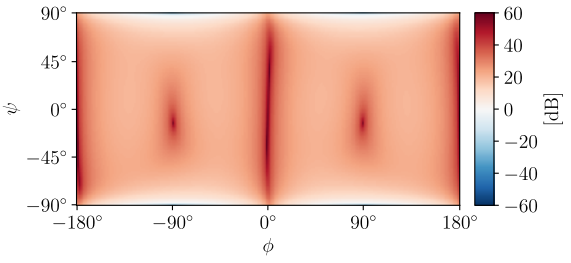

(b) XPI.

FIGURE 2. Wearable antenna radiation characteristics in free space at 4 GHz.

The antenna simulations were performed with CST Studio Suite [49], which uses the Finite Integration Technique

(FIT) method for EM field calculations. The on-body antenna characteristics were obtained with the biological voxel model Gustav, having a resolution of $2.08 \times 2.08 \times 2\,\text{mm}^3$ [50]. Three different wearable antenna locations are considered, namely, torso (TO), wrist (AL), and lower leg (LL). The number of mesh cells for the torso, leg, and hand models are 432 million, 311 million and 56 million, respectively. To reduce the computation time, given the large number of mesh cells, the simulation files were optimized for parallel processing by 5 - 10 cluster nodes with the Intel(R) Xeon(R) CPU E5-2640 v4. The corresponding body phantoms used in numerical simulations are shown in Fig. 3. In order to investigate the impact of the body-proximity on radiation characteristics, antenna-body distances of 2, 4, 6, 8, 12 and 20 mm were considered, assuming only air in the gap.

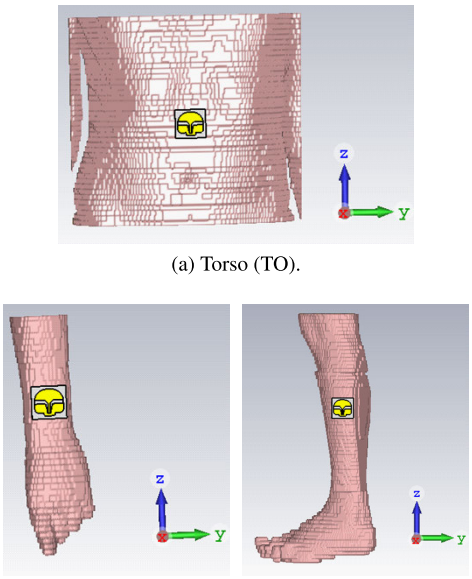

(a) Torso (TO).

(b) Wrist (AL). (c) Lower leg (LL).

FIGURE 3. Torso, hand, and lower leg phantoms extracted from the Gustav voxel model.

These distances were chosen to cover the range of typical applications and deployment scenarios. For wearable devices developed in the form of a wrist watch or a bracelet, the antenna is at a short distance from the body, i.e. between 2 and 4 mm. On the other hand, if devices are attached to the clothes, this separation tends to be larger, e.g. from 12 mm for antenna on the sleeve of a jacket, to 20 mm on the leg of a pair of trousers, or higher in the case of a dress. Furthermore, the antenna-body separation in real employments varies over time. While in some cases one might expect the distance to remain fixed during motion, e.g. bracelets or watches with tight wrist bands, distance variations are large when the devices are embedded in clothes. Therefore, the antenna separations considered in this work are selected to accommodate all these variations.

It is important to point out that the body influence on the design of the antenna adopted in this article were considered in some previous studies. The impact on the antenna matching was investigated in [10], [11], for antenna-body distances between 0 and 30 mm. A strong antenna mismatch is observed for short distances below 8 mm, while the body influence is reported to be negligible for those beyond 18 mm. This work is extended by considering implications on on- and off-body channels in [12], where antenna-body separations larger than 10 mm are recommended to avoid the excessive attenuation introduced by the body.

C. OFF-BODY CHANNEL

The impact of the user's body on off-body radio channel characteristics is analyzed by employing a previously developed channel model [38]. The model is based on geometrical optics and takes the polarization aspect of the channel and the influence of user's motion into account. Only the direct path propagation between the transmitter (Tx) and receiver (Rx) is considered in this work, in order to focus on the impact of the user's body and motion on the individual signal components. These effects are the same for the scattered signal components, which exhibit additional attenuation and depolarization associated with the particular propagation mechanism [38, Sec. III].

Based on the adopted model, the power at the Rx antenna output is obtained according to:

$$P_r = \frac{1}{2}\left|\frac{\lambda}{4\pi r}\,\mathbf{g}_{r\,[1\times 2]}^{H}\,\mathbf{Q}(\theta_{LoS})_{[2\times 2]}\,\mathbf{g}_{t\,[2\times 1]}\right|^2 \qquad (11)$$

where:

λ	wavelength;
r	Line-of-Sight (LoS) length;
$\mathbf{g}_{t/r}$	polarimetric gain vector of the Tx/Rx antenna;
$\mathbf{Q}$	rotation matrix;
θ_{LoS}	LoS mismatch angle;
$(\,.\,)^H$	Hermitian (conjugate) transpose.

The antenna radiation characteristics are represented by the polarimetric gain vectors, with complex-valued components in the orthogonal polarizations, i.e. V and H. Gain vectors are extracted from the simulated gain patterns described in the previous section. The rotation matrix in (11) represents signal depolarization due to physical misalignment between the antennas, and the mismatch angle corresponds to the angle between the polarization reference directions, i.e. $\mathbf{u}_\theta$ and $\mathbf{u}_\phi$, of the Tx and Rx antennas in the LoS direction [38].

To take the influence of user's motion into account, a mobility model for wearable antennas on dynamic users is adopted [51]. The model represents motion as a superposition of the user's linear forward motion with a periodic component associated with the dynamic posture. The periodic antenna displacement and rotation during the motion cycle, represented by Euler angles, are modeled via Fourier series with up to two harmonics. The model parameters are calculated from high-resolution Motion Capture (MoCap) data, being summarized in [51, Tab. 1].

The impact of wearable antenna motion on the channel is multifold. The antenna displacement yields a variable gain and polarization of an Multipath Component (MPC) due

to time-variant directions of departure/arrival (DoD/DoA), while its rotation due to the dynamic posture has the dominant impact on the polarization mismatch losses [39].

In order to observe how changes in wearable antennas' radiation characteristics affect the communications channel, the channel model is used to simulate a simple free space quasi-dynamic off-body communications scenario. As illustrated in Fig. 4, the user is walking or running in place, at a fixed 4 m distance from an off-body Access Point (AP), placed at a 1.5 m height. An ideal V-polarized isotropic radiator is assumed for the off-body antenna, in order to focus on the effects associated with the wearable one.

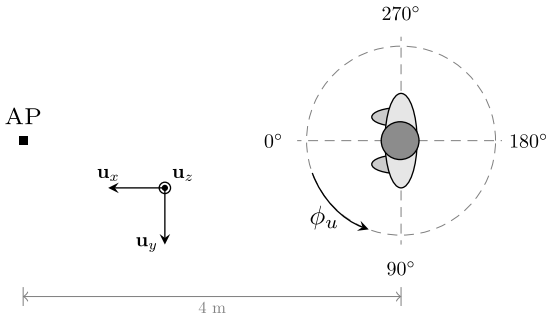

FIGURE 4. Scenario geometry.

Four user orientations are considered, namely, facing towards and away from the AP ($\phi_u = 0°, 180°$) and with either side turned towards it ($\phi_u = 90°, 270°$). These orientations correspond to different body-shadowing conditions, including unobstructed, partially or fully obstructed LoS. Simulations were repeated for the three on-body antenna locations for which the wearable antenna radiation patterns were simulated (Fig. 3). It is important to note that the considered wearable antennas yield LoS and Non-LoS (NLoS) conditions for different user orientations in Fig. 4. For example, the LoS is unobstructed for $\phi_u = 0°$ in the TO antenna case, while the same condition occurs for $\phi_u = 270°$ with the AL and LL antennas. Due to the periodic behavior of the channel, only one motion cycle is simulated, and the temporal variation of the Rx power is analyzed.

III. ANTENNA EFFICIENCY DEGRADATION

The influence of the body on the UWB antenna's radiation efficiency is investigated in this section. The S_{11} parameter is analyzed over the frequency band between 1 and 6 GHz, for antenna-distances of 2, 4, 6, 8, 12 and 20 mm, and on-body antenna locations on the TO, AL and LL. The absolute and relative S_{11} values, calculated according to (3), are shown in Fig. 5. By comparing the S_{11} curves obtained with the phantom (solid line) against the free space case (dashed line) in Fig. 5a, one observes the significant impact of the user's body on the radiation efficiency. In the proximity of the body, the resonant frequency is observed to shift and higher S_{11} values are obtained than in the free space case, thus, worse matching, particularly at shorter antenna-body distances.

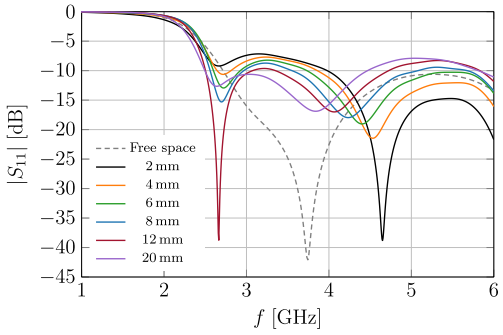

(a) S_{11} vs. frequency (TO antenna).

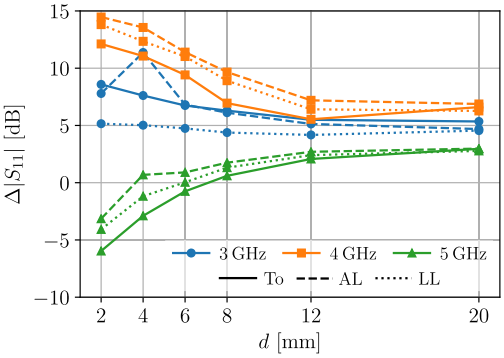

(b) ΔS_{11} vs. antenna-body distance.

FIGURE 5. Antenna input reflection coefficient S_{11} (with respect to the case with the antenna in free space).

The resonant frequency in free space is at 3.8 GHz, whereas S_{11} is observed to have two local minima for the antenna on the body (i.e. TO), albeit with significantly higher values than in free space. While one of the resonant frequencies is fixed at 2.8 GHz, the other one varies between 3.8 and 4.8 GHz, with the higher frequencies observed when the antenna is closer to the body. The lower minima at 2.8 GHz is characterized by lower input impedance mismatch losses in most cases, except for the shortest distance one, i.e. 2 mm. By taking a -10 dB threshold for the definition of the antenna bandwidth, one finds that distance has quite an impact not only on the resonant frequency but also on the bandwidth. The absolute S_{11} exhibits a similar behavior for the AL and LL antenna locations (not shown), with the exception that the second minimum is stronger in the TO case.

The relative S_{11} parameters are shown as a function of the distance in Fig. 5b. The difference between the values obtained for the three locations is considerable for short antenna-body distances, at all frequencies, while it becomes negligible for larger separations from the body. The difference between the ΔS_{11} values across the antenna locations at shorter distances is explained by the different dielectric characteristics of the body tissues on the chest, e.g. the thicknesses of the fat and muscle layers are different at TO, AL and LL. Additionally, the difference in shapes of body parts has an impact as well. By considering the AL and LL antennas, one concludes that the body proximity results in

antenna de-tuning towards a lower resonance frequency as stated earlier. The two placements yield similar results, with the corresponding S_{11} curves exhibiting the same trend.

In comparison with the free space case, the S_{11} values with the antenna on the phantom are higher, hence, additional losses due to input impedance mismatch are introduced. At 3 GHz, these losses are between 4 and 9 dB for the TO placement, 5 to 11 dB for the AL one, and between 4 and 5 dB for the LL position, with the higher losses being obtained for shorter distances. The input reflection losses are higher at 4 GHz, i.e. up to 14 dB, which is due to the proximity to the resonant frequency of the antenna in free space, where its efficiency is high. For the TO and AL placements, at 5 GHz the additional input reflection losses are below 3 dB, with the antenna efficiency for some distances below 6 mm being even better than in free space. On the other hand, the LL placement yields considerably worse antenna efficiency, with the additional impedance mismatch losses between 8 and 15 dB, the lower values being observed for shorter distances.

IV. ANTENNA RADIATION PATTERN DISTORTION

In addition to body-coupling influence on the antenna's input impedance and radiation efficiency, the user's body also distorts the shape of the radiation pattern as energy propagation behind the body is obstructed. This effect is observed in Fig. 6, showing the V- and H-polarization gain patterns obtained with several antenna distances from the torso.

By considering the free space gain pattern (black) as the reference, the body-shadowing effect is evident. The signal attenuation is found to exceed 20 dB in the shadowed region, behind the user's body, with losses increasing as the antenna gets closer to the body. A similar trend is observed for the AL and LL cases, yet the losses are found to be lower and the shadowing zone narrower, which can be attributed to the smaller relative cross-sections of arms and legs, yielding stronger fields diffracted around the body, as predicted by diffraction theories [52]. Furthermore, one can see that the antenna radiates a nearly V-polarized field in free space, while the polarization deviates towards an inclined elliptical one when placed near the body.

The body-shadowing effect is observed to change with frequency, with the higher frequencies yielding higher losses and more back-lobes in the shadowed region. The appearance of multiple radiation nulls in the directions behind the body can be associated with the interference of body-diffracted fields, traveling around the opposite sides of the body. This effect has been widely observed in previous studies, and explained by the Uniform Theory of Diffraction (UTD) and creeping wave propagation around curved/cylindrical surfaces [53], [54].

For a better insight into the overall gain characteristics, the spherical CDF of the antenna gain is calculated according to (6). By comparing the values obtained for the antenna in free space and on the body, the spherical CDF gives an insight into the body influence on the overall radiation characteristics.

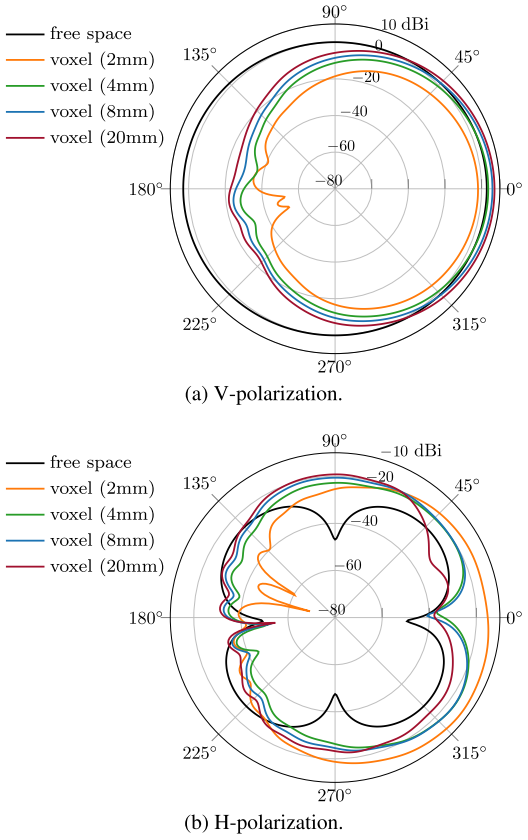

FIGURE 6. Azimuth plane gain patterns in the V- and H-polarizations for the antenna on the torso, with different distances, at 3 GHz.

Fig. 7 shows the CDF obtained at 3 GHz, for the TO antenna with different separations from the body. This case is chosen for illustration, but one should note that the same general trend is found for all considered antenna placements and carrier frequencies. The body proximity apparently results in low gain over a significantly larger spherical area than in the free space case, with shorter distances yielding lower gain. For example, by considering a -10 dBi threshold, the lower antenna gain values are found over less than 4% of spherical area in the free space case, while this area is more than 50% for the 20 mm distance and more than 70% for the 2 mm one in the on-body case. This shows that the stronger body-coupling and body-shadowing effects closer to the body result in reduced radiation efficiency. However, the on-body antenna gain also improves in some directions; while the maximum gain in free space is 2.5 dBi, the higher gain is observed for 15% of the spherical area with distances of 12 and 20 mm. This is a result of body-reflected signals, which add up constructively to yield effectively higher gain in the direction away from the body.

The influence of antenna placement and carrier frequency can be observed in Fig. 8, which shows the CDF for an antenna-body distance of 4 mm (other distances show similar trends). The difference between antenna locations is once more apparent. The TO placement yields lower gain over a larger portion of the radiation sphere than the other two,

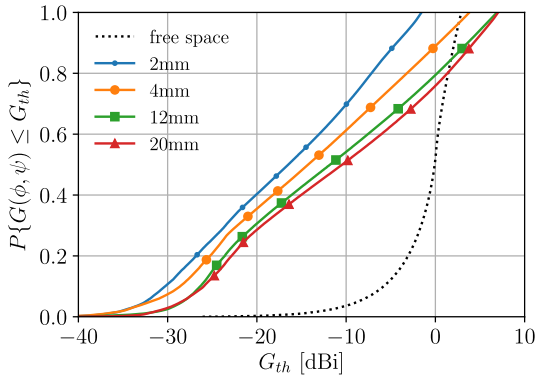

FIGURE 7. Gain CDF for the TO antenna at 3 GHz, with different antenna-body distances.

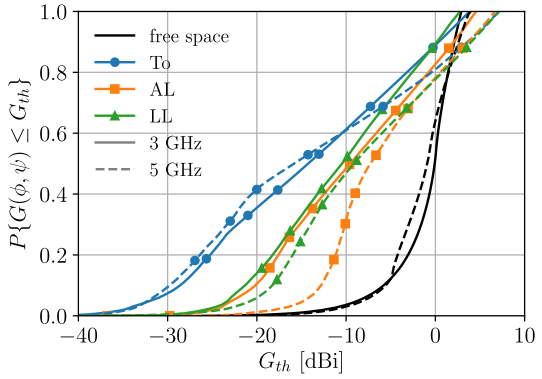

FIGURE 8. Gain CDF for different antenna locations and carrier frequencies, for 4 mm distance.

which is attributed to the stronger shadowing effect from the torso. For comparison, at 3 GHz the portion of the spherical area with gain below -20 dBi is around 40% for the TO case, while being around 10% for AL and LL ones. For the reference, this area is negligible in the free space case. The median gain, with 50% of the spherical area being with the lower/higher values, is around -15 dBi for TO, and -10 dBi for AL and LL, while being around 0 dBi in free space.

The difference in the results obtained at different frequencies is quite low for the free space case, while being more significant for the antenna on the body. In the TO case, the CDF curve for 5 GHz is slightly above the 3 GHz one at lower gains, while being below it and reaching further right at higher gain values; the former behavior is explained by higher body-shadowing losses at 5 GHz, while the latter is associated with the focusing effect of body-reflections, yielding a higher gain in the direction away from the body. On the other hand, the CDF at 5 GHz is consistently below the 3 GHz one for AL and LL, with the difference being particularly notable for the former placement. While body-reflections play a similar role herein as in the previous case for higher gain values, the lower CDF values at low gains observed at the higher frequency are somewhat surprising. Further inspection of the gain patterns shows that the H-polarization gain in the shadow region is higher at 5 GHz for this antenna placement, which points out to stronger excitation of creeping waves as a potential reason for this result. This observation is further discussed in the following Section V.

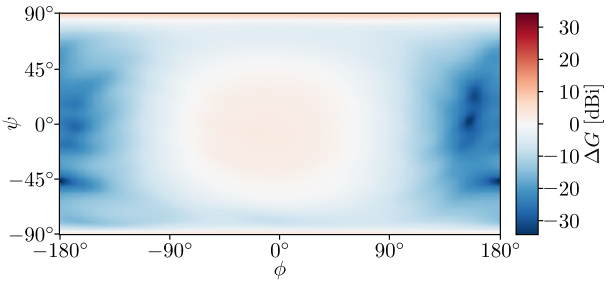

FIGURE 9. Gain difference for LL antenna at 3 GHz, for 12 mm antenna-body distance.

A better insight into the body influence can be obtained by analyzing how much the gain changes relative to the free space case. For example, Fig. 9 shows the gain difference at 3 GHz for the LL antenna at 12 mm from the body, i.e. calculated according to (4), where the symmetrical colormap is used to easily identify the areas where the antenna gain decreases (blue), increases (red), or remains the same as in free space (white). The dominant blue areas show reduced radiation, especially in the directions towards the body ($\pm 180°$), where body-shadowing losses are higher. On the other hand, the light red tones show improved gain in the directions away from the body, where body-reflections effectively focus the radiated energy. The antenna gain is also observed to improve at poles, as indicated by the red strips at elevation angles $\pm 90°$. This is due to the softening of the radiation nulls, as the doughnut shape of the radiation pattern distorts towards a hemispherical one. It is noteworthy that these effects are observed at all considered frequencies and on-body locations, however, with differences in intensity of the shadowing in the back and the gain improvement in the forward direction.

In order to investigate these two observed effects better, the radiation sphere is partitioned into two regions defined in (7) and (8), corresponding to the directions in which the antenna gain on the body is higher/lower than in free space $\mathcal{R}_{\pm}(\Delta G)$. The two regions are complementary, being irregularly shaped and discontinuous in general, as it can be observed in Fig. 9, where the red tones corresponding to $\mathcal{R}_{\pm}(\Delta G)$ are found in the forward direction around $\phi, \psi = 0°$, but also at the poles. The size of the two regions and gain statistics provide a quantitative measure of the overall body effects on the antenna gain pattern.

Fig. 10 shows the portion of the total spherical area corresponding to $\mathcal{R}_{+}(\Delta G)$, which is observed to increase with distance; note that $\mathcal{R}_{-}(\Delta G)$ decreases at the same rate. At 3 GHz, this region accounts for less than 3% of the total sphere at 2 mm, while being around 30% at 20 mm, with a similar behavior observed for all on-body placements. The existence of a non-zero albeit small area of $\mathcal{R}_{+}(\Delta G)$, even with the strong body coupling at 2 mm is not surprising, and

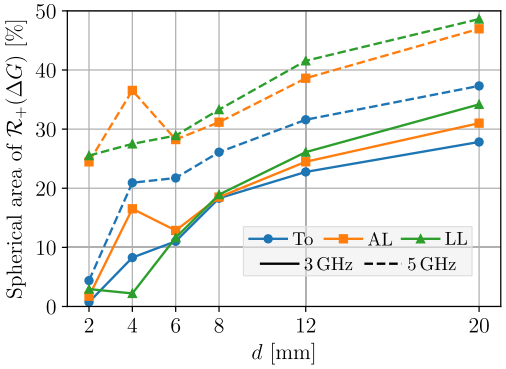

FIGURE 10. Fraction of the total radiation sphere area corresponding to $\mathcal{R}_+(\Delta G)$.

can be associated with dampening of the radiation nulls at poles when the antenna is placed on the body.

The area of $\mathcal{R}_+(\Delta G)$ is larger at 5 GHz, increasing from more than 25% at 2 mm to almost 50% at 20 mm (i.e. for AL and LL antennas), with the relative change following almost identical trend as at 3 GHz. This trend in frequency can be interpreted in the same way as the one with distance, since the same physical distances are electrically longer at higher frequencies. The difference in the size of $\mathcal{R}_+(\Delta G)$ between TO and the other two antenna locations is more significant at 5 GHz, especially for 2 mm, where the area is around five times smaller for the TO case. This is likely explained by stronger body-shadowing from the torso, but also coupling effects being greatly affected by the body tissue type at each on-body location.

Fig. 11 shows the gain difference statistics over the regions $\mathcal{R}_\pm(\Delta G)$, namely, the mean and standard deviation calculated according to (9) and (10), respectively. The average gain difference over $\mathcal{R}_+(\Delta G)$ is consistently around 2 dB for all distances, with some deviations from this value observed only for shorter distances at 3 GHz. By considering that the area of $\mathcal{R}_+(\Delta G)$ is less than 3% of the total sphere at this frequency (Fig. 10), being concentrated around the poles in this case, this slightly higher gain can be explained by the previously mentioned softening of the radiation nulls in the proximity of the body tissue. On the other hand, the average gain difference over $\mathcal{R}_-(\Delta G)$ is around -10 dB for AL and LL antennas, and -15 dB for the TO one, over all distances. These negative values are associated with the body-shadowing effect, which is observed to be stronger for the TO than for the other two antennas.

By considering the corresponding standard deviation, one finds considerably higher values for $\mathcal{R}_-(\Delta G)$ than for $\mathcal{R}_+(\Delta G)$. This is expected as the range of the negative gain difference values is much wider than the positive ones, being below 10 dB in most cases. Based on the same reasoning, the approximately 3 dB higher standard deviation obtained for the TO antenna compared with the other two in $\mathcal{R}_-(\Delta G)$ is explained by the stronger shadowing from the torso, which contributes to the further range extension of the negative gain difference values in this region.

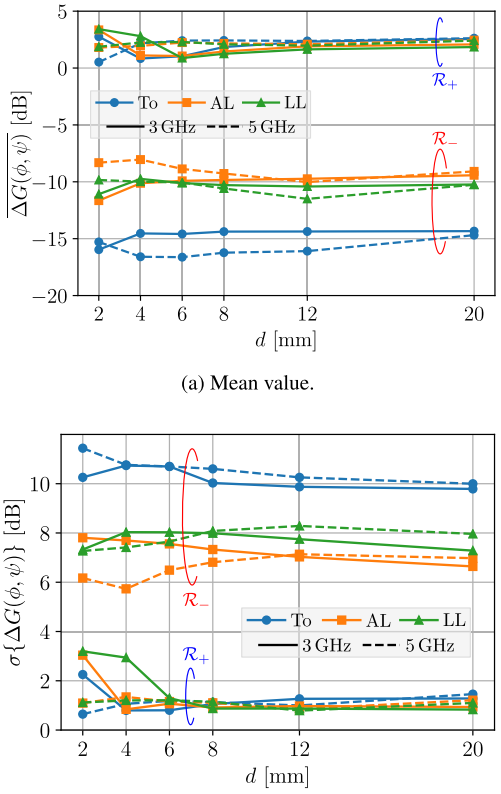

(a) Mean value.

(b) Standard deviation.

FIGURE 11. Gain difference statistics within $\mathcal{R}_\pm(\Delta G)$.

V. ANTENNA DEPOLARIZATION

Antenna depolarization is the least investigated aspect of the body influence on wearable antennas, while it can have a detrimental effect on the channel. This effect is illustrated in Fig. 12, showing polarization ellipses scaled according to the corresponding gain, for a few selected azimuth directions. The axes ratio and inclination of the principal axes show the antenna polarization in the indicated direction, while the ellipses' sizes correspond to the gain, normalized to the maximum value.

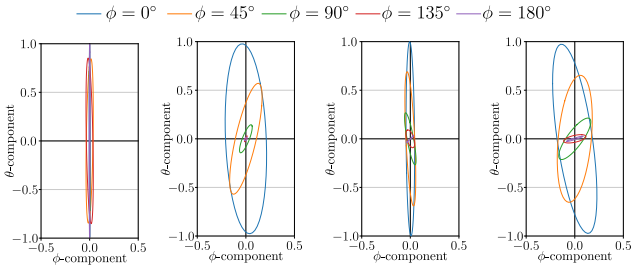

(a) Free space. (b) TO antenna. (c) AL antenna. (d) LL antenna.

FIGURE 12. Polarization ellipses normalized by the antenna gain for the selected azimuth directions (3 GHz, 2 mm antenna-body distance).

As one observes from Fig. 12, in free space the antenna is V-polarized in all considered directions. When operating near the body, the polarization is seen to change from a linear to an

elliptical one, with different inclinations of the principal axis observed in different azimuth directions. Therefore, the polarization of the antenna changes as one moves from the main off-body direction ($\phi_u = 0°$), i.e. where it is V, to a more elliptical and almost orthogonally inclined one in the shadow area behind the body. Body-shadowing losses are apparent in these graphs as well, where polarization ellipses are significantly smaller in the back-radiation direction, compared to the forward one.

By adopting a similar approach used to evaluate the impact on the antenna gain in Section IV, the spherical CDF of the antenna XPI is used to evaluate the depolarization effect. It is calculated as the ratio of the spherical area over which XPI is below a given value and the total sphere area (Section II-A). This CDF can be used to evaluate the body influence by comparing results obtained with different antenna-body distances.

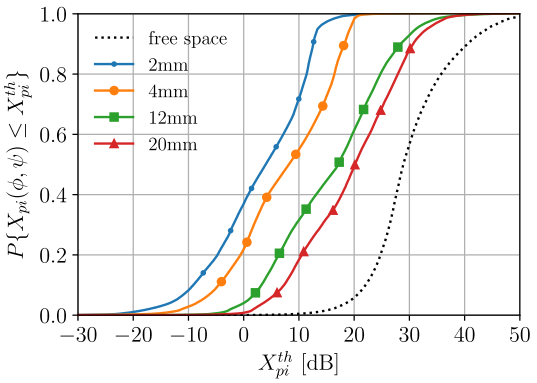

FIGURE 13. XPI CDF for the LL antenna at 3 GHz, with different distances.

Fig. 13 presents such a comparison by considering the LL antenna at 3 GHz (the other cases show similar results). The body influence is apparent, as the CDF curves obtained for the shorter distances are consistently shifted to the left from the one obtained for the free space case. This means that the operation closer to the body yields a higher degree of antenna depolarization, with lower XPI characterizing larger portions of the radiation sphere. The antenna XPI in free space is above 10 dB over more than 99% of the radiation sphere, hence, being mostly V-polarized in this case, as previously observed in Fig. 2b.

On the other hand, when the antenna is on the body, the corresponding area is around 20% at 20 mm, 35% at 12 mm, 55% at 4 mm, and up to 70% at 2 mm distance. Furthermore, by considering the CDF value at 0 dB as an indicator of the portion of the radiation sphere with the antenna polarization being more inclined towards H than V, the figure shows that while this fraction is less than 1% at 20 mm distance, it is around 5% at 12 mm, 21% at 4 mm and almost 40% at 2 mm.

The impact of the carrier frequency and on-body location on the antenna polarization characteristics can be observed from Fig. 14, showing the spherical CDF of XPI for a fixed distance of 4 mm (similar results are obtained for other cases). The higher frequency is observed to yield a higher level of depolarization, with the spherical area assuming high XPI being reduced while the range of values is generally preserved, resulting in steeper CDF curves at 5 GHz. This is most notable in the free space case, where the median value is around 10 dB lower at 5 GHz than 3 GHz. This trend with frequency is observed to vary between antenna locations.

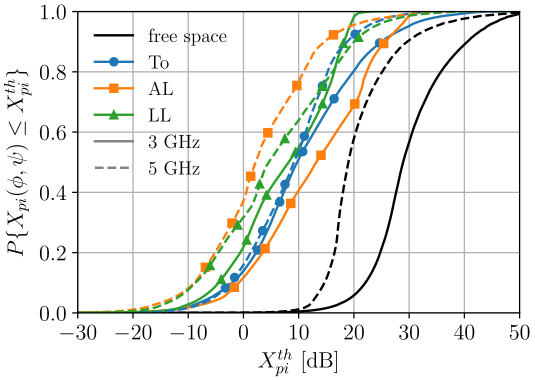

FIGURE 14. XPI CDF for different antenna locations and carrier frequencies, for 4 mm distance.

As in the previous section, the body influence is best observed by comparing the antenna characteristics on the body against those in free space. Fig. 15 shows the XPI difference at 3 GHz for the TO antenna at 2 mm from the body, calculated as described in Section II-A. A symmetrical colormap is adopted for this case as well, where the blue/red tones correspond to directions with the on-body antenna XPI being lower/higher than in the free space case, respectively.

The figure shows a high degree of depolarization, as the intensive blue areas indicate a significant deviation from the V polarization obtained in free space. The more intensive depolarization is observed in directions behind the body, where the XPI difference below -25 dB implies a nearly H-polarized signal. On the other hand, a small red patch around $\phi, \psi = -45°$ shows that in proximity of the body the antenna polarization inclines towards the V one in some directions. A similar trend is observed at all considered frequencies, on-body antenna locations and distances from the body.

For a better analysis of these effects, the radiation sphere is divided into two regions similarly as in Section IV, but with the two regions $\mathcal{R}_{\pm}(\Delta X_{pi})$ herein corresponding to the directions in which the on-body antenna XPI is higher/lower than in free space. Analogously, these regions are complementary, irregular and discontinuous. Their sizes and XPI statistics within provide a quantitative measure of the overall body effects on the antenna polarization characteristics.

Fig. 16 shows the portion of the total spherical area corresponding to $\mathcal{R}_{+}(\Delta X_{pi})$, which is seen to increase with distance, i.e. from less than 5% at 2 mm to up to 40% at 20 mm, the latter being observed for the LL antenna at 5 GHz. With two exceptions, the size of $\mathcal{R}_{+}(\Delta X_{pi})$ is below 10% for antenna-body distances up to 12 mm, and below 20% for the

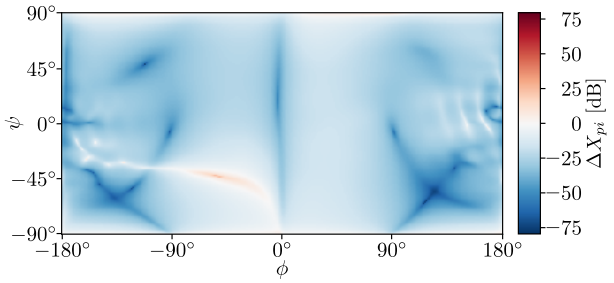

FIGURE 15. XPI difference for the TO antenna at 3 GHz, for 2 mm.

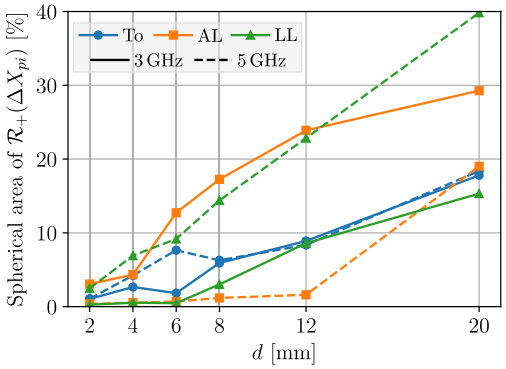

FIGURE 16. Fraction of the total radiation sphere area corresponding to $\mathcal{R}_+(\Delta X_{pi})$.

maximum one of 20 mm. However, unlike the case with the antenna gain, no consistent trends with the antenna location or frequency can be observed for the XPI difference. The change in frequency is observed to have significantly different effects on the spherical area occupied by $\mathcal{R}_+(\Delta X_{pi})$ for different antenna placements. More precisely, while this area is nearly the same at 3 GHz and 5 GHz for the TO antenna, for the AL one it is considerably larger at the lower frequency, and the opposite is observed for the LL antenna.

Fig. 17 shows the XPI difference mean and standard deviation calculated over the two regions $\mathcal{R}_\pm(\Delta X_{pi})$, as described in Section II-A. The average XPI difference over $\mathcal{R}_+(\Delta X_{pi})$ is around 4 dB for all distances, in all considered cases. On the other hand, the mean over $\mathcal{R}_-(\Delta X_{pi})$ is below -7 dB, where a minimum of -27 dB obtained for the 2 mm antenna-body separation shows a high degree of antenna depolarization. The average XPI difference over this region is seen to increase with distance and frequency, and the trend is found to be consistent for all antenna locations. This implies that stronger antenna-body coupling at electrically shorter distances results in more severe depolarization effect. The standard deviation presented in Fig. 17b shows a behavior similar to the one exhibited by the gain difference in Fig. 11b, with the apparent effect of the range of XPI difference values in each region.

VI. EFFECTS ON THE OFF-BODY CHANNEL

This section investigates the user's influence on the off-body radio channel, including the impact of the antenna radiation characteristics and the influence of user's motion through

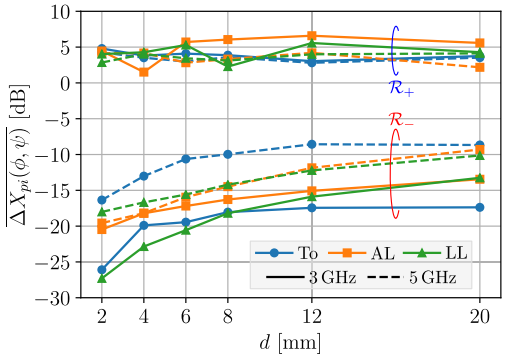

(a) Mean value.

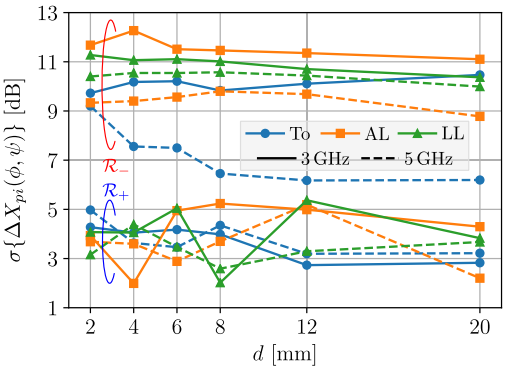

(b) Standard deviation.

FIGURE 17. XPI difference statistics within $\mathcal{R}_\pm(\Delta X_{pi})$.

antenna displacement and rotation. Results are presented for the user running at a speed of 3.55 m/s [51, Sec. III-D], where the Rx power obtained for the TO, AL and LL antenna placements is analyzed over a motion cycle.

A. ANTENNA ON THE TORSO

Among the three considered antenna placements, the TO one yields the least dynamic signal variation. For the case with the user facing towards the AP, the Rx power varies within 2 dB, which is expected as the torso is nearly static during the changes in posture. When the user faces away from the AP and obstructs the LoS, the Rx power is observed to suffer from body-shadowing losses exceeding 25 dB. In practice, this means that the communication channel conditions can change drastically, as the user simply rotates relative to the AP. This is observed in Fig. 18, which shows the Rx power over a running cycle obtained for the user turned away from the AP, with the body obstructing the direct path and yielding a NLoS condition. It is important to point out that the Rx power obtained with the antenna on the body in the LoS case, i.e. $\phi_u = 0°$, approximately matches the levels corresponding to the antenna in free space in Fig. 18; the trend is exactly matched and only a fixed offset of a few dB can be noticed due to the body effects on the antenna gain.

The signal variations obtained for the TO antenna are due to the gain variations in the LoS direction, as the antenna

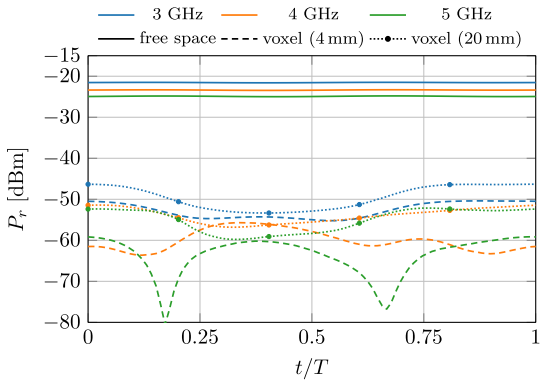

FIGURE 18. Rx power over a running cycle for the TO antenna, with $\phi_u = 180°$ (NLoS).

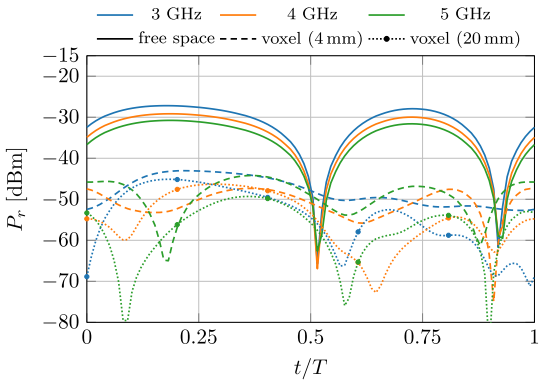

FIGURE 19. Rx power over a running cycle for the AL antenna, with $\phi_u = 90°$ (NLoS).

exhibits a periodic rotation around the vertical axis of the torso during the motion cycle. Since the user's torso remains nearly vertical, the Tx and Rx antennas' polarizations are practically matched in this case. It is important to point out that the signal variations for the TO antenna are quite similar for walking and running, being slightly less dynamic in the former case. For the two cases when the user is oriented sideways towards the AP, with the wearable antenna's maximum radiation direction being approximately orthogonal to the LoS ($\phi_u = 90°, 270°$), the Rx signal exhibits slow variations at levels in between those obtained for the LoS and NLoS cases.

B. ANTENNA ON THE WRIST

The AL antenna yields significantly larger and more dynamic Rx power variations than the TO one. This can be observed from Fig. 19, showing the Rx power over the running cycle for the case when the user is obstructing the LoS. By considering the free space case (solid lines), two distinct Rx power minima are observed during the motion cycle when the user is facing sideways towards the AP. With the hands of a running person swinging up and down, the signal variations in these figures can be associated with the polarization mismatch losses, with the observed power minima occurring when the user's hand is horizontally aligned, resulting in practically cross-polarized antennas. The antenna gain is nearly constant and has a negligible effect on the Rx power, as the LoS direction changes very little with the wearable antenna rotation in this case, being nearly aligned with the rotation axis.

The Rx signal variation is less regular for the radiation pattern obtained with the phantom (dashed lines), as its shape is not symmetric as the free-space one. However, the two cases yield overlapping results for the LoS case, i.e. $\phi_u = 270°$, since the AP is in the forward radiation direction of the wearable antenna, being least affected by the body. On the other hand, the additional shadowing loss and irregular variation due to the distorted gain pattern with the antenna on the wrist is apparent for the NLoS case in Fig. 19.

Albeit not shown, the Rx power exhibits almost identical behavior when the user is facing towards or away from the antenna, with two Rx power minima occurring around the same points in the motion cycle as in Fig. 19. However, the two minima in that case are caused by different effects. While the one near $t/T = 0.9$ is again due to the polarization mismatch loss, i.e. as the antennas' axes seen along the LoS direction get orthogonally inclined, the other minimum around $t/T = 0.5$ is caused by the antenna gain variation. More precisely, for the user's orientations $\phi_u = 0°, 180°$, the LoS direction varies around the null at the pole of the doughnut-shaped radiation pattern of the wearable antenna in free space (Fig. 2a),

One should note that the Rx signal from the AL antenna shows a significantly different behavior for the walking case, compared to the running one presented herein, the Rx power variations being much slower and with lower magnitude. This is due to the specific posture of a running person, i.e. with the lower arms being nearly horizontal, compared to their nearly vertical swinging motion in the walking case.

C. ANTENNA ON THE LOWER LEG

The Rx power obtained with the LL antenna is observed to exhibit a similar behavior over the motion cycle as in the AL antenna case, as one can observe from Fig. 20. For the free space radiation pattern, two deep signal fades are observed for all four considered orientations of the user. For the user oriented sideways with respect to the AP, i.e. $\phi_u = 90°, 270°$, the Rx power minima occur due to polarization mismatch losses as the Tx and Rx antennas' physical inclinations become nearly orthogonal, while the wearable antenna gain remains constant and has no effect on the observed signal behavior. By considering the radiation pattern obtained with the phantom, in the LoS case ($\phi_u = 270°$) one again finds the same signal behavior as when the free space radiation pattern is used. On the other hand, apparently more random signal variations and body-shadowing losses exceeding 20 dB are observed for the case with the AP being in the shadowed zone (Fig. 20).

For the user facing towards or away from the off-body antenna (not shown here), i.e. $\phi_u = 0°, 180°$, the Rx power minima are explained by the variable gain in the LoS

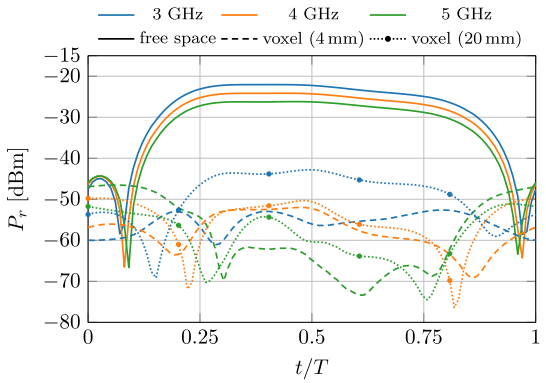

FIGURE 20. Rx power over a running cycle for the LL antenna, with $\phi_u = 90°$ (NLoS).

direction, as it aligns with the radiation nulls at the poles as the user's legs swing between the foot-ground contacts. The antennas' vertical axes practically remain within the same (vertical) plane, thus their polarizations being matched and no mismatch losses occur.

For the walking case, the Rx signal from the LL antenna exhibits much less dynamic variation than observed for the running one presented herein. However, the signal variations for this antenna placement are considerably more severe than for the TO and AL antennas, with the difference being much more striking in the walking case.

By comparing the results obtained with antenna-body distances of 4 mm and 20 mm, the shorter distance is observed to yield lower Rx power levels in almost all cases. This is explained by the stronger body coupling effects on the antenna radiation characteristics when the antenna is closer to the body (Sections III-V). On the other hand, the lower Rx power obtained at higher frequencies is explained by the higher free space path loss, as well as higher diffraction losses when the LoS is obstructed.

VII. CONCLUSION

With the growing interest for BAN applications in various fields, the understanding of body-centric radio propagation is increasingly important, as the system's performance is strongly determined by the communications quality. The effects of the user's body on the wearable antenna radiation characteristics and the impact of motion on the Rx signal are the major aspects to which a considerable research effort has already been dedicated. However, the polarization aspect of BAN radio channels and the signal depolarization within are mostly neglected in literature.

By considering a UWB wearable antenna, this work investigates the influence of the user's body on wearable antenna radiation characteristics at 3, 4 and 5 GHz, for placements on the torso, wrist and lower leg, with different antenna-body separations. The analysis is based on EM simulations with numerical phantoms, and its focus is on the imposed body-shadowing losses and antenna depolarization. The simulated antenna gain patterns are then employed in dynamic off-body channel simulations using a previously developed polarized channel model.

Results show a strong influence of the body on the antenna radiation characteristics, with the shorter antenna-body distances yielding more severe effects on the input impedance, gain and polarization. The resonant frequency changes compared to the free space case, and the input reflection coefficient is generally higher over the considered frequency band. Similarly, the spatial gain distribution is distorted and radiation in the shadowed zone behind the body is suppressed, with the body-shadowing losses exceeding 20 dB. Due to the stronger shadowing, the signal attenuation by the torso is higher than from the wrist and lower leg. The gain is also seen to slightly improve in some directions, due to body reflections. The antenna polarization is observed to change from a linear vertical one in free space, to an elliptical one when the other antenna is placed on the body.

The off-body channel simulations show strong effects of the body shadowing and polarization mismatch on the Rx power, and the wearable antenna rotation during motion has a crucial impact. The signal variation dynamics greatly depend on the on-body antenna location, where the arm and lower leg placements yield significantly more dynamic channel conditions than the torso. The polarization mismatch losses due to physical misalignment of the antenna during a motion cycle yield more than 30 dB LoS component power fades, effectively changing the channel conditions from LoS to NLoS, while the direct path is physically unobstructed.

In order to further investigate the influence of the user's body and motion on off-body channel characteristics in more realistic conditions, future work will address a multipath propagation scenario, taking the signal depolarization effect due to scattering mechanisms into account as well. Moreover, other antenna designs will be considered to evaluate their sensitivity to the effects observed in this article.

ACKNOWLEDGMENT

The research at IST was performed within the framework of the COST Action CA15104, IRACON.

REFERENCES

[1] (2019). *United Nations: Department of Economic and Social Affairs, World Population Ageing*. Accessed: Feb. 2020. [Online]. Available: https://www.un.org/en/development/desa/population/publications/pdf/ageing/WorldPopulationAgeing2019-Highlights.pdf

[2] H. B. Lim, D. Baumann, J. Cai, R. Koh, E. P. Li, and Y. Lu, "Antennae polarization for effective transmission of UWB signal around human body," in *Proc. IEEE Int. Conf. Ultra-Wideband*, Singapore, Sep. 2007, pp. 220–224.

[3] Y.-L. Zheng, X.-R. Ding, C. C. Y. Poon, B. P. L. Lo, H. Zhang, X.-L. Zhou, G.-Z. Yang, N. Zhao, and Y.-T. Zhang, "Unobtrusive sensing and wearable devices for health informatics," *IEEE Trans. Biomed. Eng.*, vol. 61, no. 5, pp. 1538–1554, May 2014.

[4] (Dec. 2019). *Bluetooth Core Specification, v5.2*. Accessed: Jun. 2020. [Online]. Available: https://www.bluetooth.org/docman/handlers/downloaddoc.ashx?doc_id=478726

[5] *IEEE Standard for Information Technology–Telecommunications and Information Exchange Between Systems Local and Metropolitan Area Networks'Specific Requirements—Part 11: Wireless LAN Medium Access Control (MAC) and Physical Layer (PHY) Specifications*, IEEE Standard 802.11-2016 and 802.11-2012, Dec. 2016, pp. 1–3534.

[6] *IEEE Standard for Local and Metropolitan Area Networks—Part 15.6: Wireless Body Area Networks*, IEEE Standard 802.15.6-2012, Feb. 2012.

[7] *Smart Body Area Networks*. Accessed: Jun. 2020. [Online]. Available: https://www.etsi.org/technologies/smart-body-area-networks

[8] T. S. P. See, Z. N. Chen, and X. M. Qing, "Proximity effect of UWB antenna on human body," in *Proc. Asia Pacific Microw. Conf.*, Singapore, Dec. 2009, pp. 2192–2195.

[9] T. S. P. See and Z. N. Chen, "Experimental characterization of UWB antennas for on-body communications," *IEEE Trans. Antennas Propag.*, vol. 57, no. 4, pp. 866–874, Apr. 2009.

[10] T. Kumpuniemi, M. Hämäläinen, K. Y. Yazdandoost, and J. Iinatti, "Human tissue type and volume effect on the on-body UWB antenna matchings," in *Proc. 10th Int. Symp. Med. Inf. Commun. Technol. (ISMICT)*, Worchester, MA, USA, Mar. 2016, pp. 1–5.

[11] T. Tuovinen, T. Kumpuniemi, K. Y. Yazdandoost, M. Hämäläinen, and J. Iinatti, "Effect of the antenna-human body distance on the antenna matching in UWB WBAN applications," in *Proc. 7th Int. Symp. Med. Inf. Commun. Technol. (ISMICT)*, Tokyo, Japan, Mar. 2013, pp. 193–197.

[12] T. Tuovinen, T. Kumpuniemi, M. Hämäläinen, K. Yekeh Yazdandoost, and J. Iinatti, "Effect of the antenna-body distance on the on-ext and on-on channel link path gain in UWB WBAN applications," in *Proc. 35th Annu. Int. Conf. IEEE Eng. Med. Biol. Soc. (EMBC)*, Osaka, Japan, Jul. 2013, pp. 1242–1245.

[13] M. Särestöniemi, C. Kissi, C. P. Ráez, M. Hämäläinen, and J. Iinatti, "Impact of the antenna-body distance on the WBAN channel characteristics," in *Proc. 13th Int. Symp. Med. Inf. Commun. Technol. (ISMICT)*, Oslo, Norway, May 2019, pp. 1–6.

[14] T. Tuovinen, K. Yekeh Yazdandoost, M. Berg, and J. Iinatti, "Ultra wideband loop antenna on contact with human body tissues," *IET Microw., Antennas Propag.*, vol. 7, no. 7, pp. 588–596, May 2013.

[15] T. S. P. See, T. M. Chiam, M. C. K. Ho, and M. R. Yuce, "Experimental study on the dependence of antenna type and polarization on the link reliability in on-body UWB systems," *IEEE Trans. Antennas Propag.*, vol. 60, no. 11, pp. 5373–5380, Nov. 2012.

[16] M. Koohestani, J.-F. Zurcher, A. A. Moreira, and A. K. Skrivervik, "A novel, low-profile, vertically-polarized UWB antenna for WBAN," *IEEE Trans. Antennas Propag.*, vol. 62, no. 4, pp. 1888–1894, Apr. 2014.

[17] Y. I. Nechayev, X. Wu, C. C. Constantinou, and P. S. Hall, "Effect of body motion on propagation path gain at 60 GHz," in *Proc. 6th Eur. Conf. Antennas Propag. (EUCAP)*, Prague, Czech Republic, Mar. 2012, pp. 3397–3401.

[18] P. S. Hall, "Antennas and propagation for body centric communications," in *Proc. IET Seminar Antennas Propag. Body-Centric Wireless Commun.*, Nice, France, 2007, pp. 1–7.

[19] P. S. Hall, Y. Hao, V. I. Necha, A. Alomain, C. C. Constantinou, C. Parini, M. R. Kamarudin, T. Z. Salim, D. T. Heel, R. Dubrovka, A. S. Owadall, W. Song, A. Serra, P. Nepa, M. Gaio, and M. Bozzetti, "Antennas and propagation for on-body communication systems," *IEEE Antennas Propag. Mag.*, vol. 49, no. 3, pp. 41–58, Jun. 2007.

[20] G. A. Conway and W. G. Scanlon, "Antennas for over-body-surface communication at 2.45 GHz," *IEEE Trans. Antennas Propag.*, vol. 57, no. 4, pp. 844–855, Apr. 2009.

[21] S. Dumanli, "On-body antenna with reconfigurable radiation pattern," in *IEEE MTT-S Int. Microw. Symp. Dig.*, London, U.K., Dec. 2014, pp. 1–3.

[22] Z. Ning Chen, A. Cai, T. S. P. See, X. Qing, and M. Y. W. Chia, "Small planar UWB antennas in proximity of the human head," *IEEE Trans. Microw. Theory Techn.*, vol. 54, no. 4, pp. 1846–1857, Jun. 2006.

[23] M. Klemm and G. Troester, "EM energy absorption in the human body tissues due to UWB antennas," *Prog. Electromagn. Res.*, vol. 62, pp. 261–280, 2006.

[24] S. L. Cotton, A. McKernan, A. J. Ali, and W. G. Scanlon, "An experimental study on the impact of human body shadowing in off-body communications channels at 2.45 Ghz," in *Proc. 5th Eur. Conf. Antennas Propag. (EuCAP)*, Rome, Italy, Apr. 2011, pp. 3133–3137.

[25] R. Dautov and G. R. Tsouri, "Dynamic off-body Rician channel modeling for indoor wireless body area networks," *IEEE J. Biomed. Health Informat.*, vol. 24, no. 5, pp. 1246–1254, May 2020.

[26] K. Zhao, S. Zhang, Z. Ho, O. Zander, T. Bolin, Z. Ying, and G. F. Pedersen, "Spherical coverage characterization of 5G millimeter wave user equipment with 3GPP specifications," *IEEE Access*, vol. 7, pp. 4442–4452, Dec. 2019.

[27] I. Syrytsin, S. Zhang, G. F. Pedersen, K. Zhao, T. Bolin, and Z. Ying, "Statistical investigation of the user effects on mobile terminal antennas for 5G applications," *IEEE Trans. Antennas Propag.*, vol. 65, no. 12, pp. 6596–6605, Dec. 2017.

[28] V. Raghavan, S. Noimanivone, S. Kil Rho, B. Farin, P. Connor, R. A. Motos, Y.-C. Ou, K. Ravid, M. Ali Tassoudji, O. H. Koymen, and J. Li, "Hand and body blockage measurements with form-factor user equipment at 28 GHz," 2019, *arXiv:1912.03717*. [Online]. Available: http://arxiv.org/abs/1912.03717

[29] T. Uusitupa and T. Aoyagi, "Analysis of dynamic on-body communication channels for various movements and polarization schemes at 2.45 GHz," *IEEE Trans. Antennas Propag.*, vol. 61, no. 12, pp. 6168–6179, Dec. 2013.

[30] T. Tuovinen, M. Berg, K. Yazdandoost, E. Salonen, and J. Iinatti, "Radiation properties of the planar UWB dipole antenna in the proximity of dispersive body models," in *Proc. 7th Int. Conf. Body Area Netw.*, Oslo, Norway, 2012, pp. 82–88.

[31] M. Berg and T. Tuovinen, "Propagation along a human body surface in WBAN; remarks of desirable antenna characteristics," in *Proc. 4th Int. Conf. Wireless Mobile Commun. Healthcare Transforming Healthcare Through Innov. Mobile Wireless Technol.*, Athens, Greece 2014, pp. 324–327.

[32] T. Tuovinen, M. Berg, and E. Salonen, "The effect of antenna pattern and polarization for launching creeping waves on a skin surface," in *Proc. 8th Eur. Conf. Antennas Propag. (EuCAP)*, Apr. 2014, pp. 1743–1746.

[33] S. L. Cotton, "A statistical model for shadowed body-centric communications channels: Theory and validation," *IEEE Trans. Antennas Propag.*, vol. 62, no. 3, pp. 1416–1424, Mar. 2014.

[34] L. Vallozzi, P. Van Torre, C. Hertleer, H. Rogier, M. Moeneclaey, and J. Verhaevert, "Wireless communication for firefighters using dual-polarized textile antennas integrated in their garment," *IEEE Trans. Antennas Propag.*, vol. 58, no. 4, pp. 1357–1368, Apr. 2010.

[35] K. Turbic, S. J. Ambroziak, and L. M. Correia, "Characteristics of the polarised off-body channel in indoor environments," *EURASIP J. Wireless Commun. Netw.*, vol. 2017, no. 1, p. 174, Oct. 2017.

[36] S.-C. Kwon, G. L. Stüber, A. V. Lopez, and J. Papapolymerou, "Geometrically based statistical model for polarized body-area-network channels," *IEEE Trans. Veh. Technol.*, vol. 62, no. 8, pp. 3518–3530, Oct. 2013.

[37] S.-C. Kwon, G. L. Stüber, A. V. Lopez, and J. Papapolymerou, "Polarized channel model for body area networks using reflection coefficients," *IEEE Trans. Veh. Technol.*, vol. 64, no. 8, pp. 3822–3828, Aug. 2015.

[38] K. Turbic, L. M. Correia, and M. Beko, "A channel model for polarized off-body communications with dynamic users," *IEEE Trans. Antennas Propag.*, vol. 67, no. 11, pp. 7001–7013, Nov. 2019.

[39] K. Turbic and L. M. Correia, "Effects on polarization characteristics of off-body channels with dynamic users," in *Proc. IEEE Wireless Commun. Netw. Conf. (WCNC)*, Seoul, South Korea, May 2020, pp. 1–6.

[40] K. Turbic, M. Särestöniemi, M. Hämäläinen, T. Kumpuniemi, and L. M. Correia, "A preliminary analysis of user's body impact on signal polarization in WBANs," in *Proc. 14th Eur. Conf. Antennas Propag. (EuCAP)*, Copenhagen, Denmark, Mar. 2020, pp. 1–4.

[41] *IEEE Standard for Definitions of Terms for Antennas*, IEEE Standard 145-2013 and 145-1993, Mar. 2014.

[42] *User Equipment (UE) Radio Transmission and Reception; Part 2: Range 2 Standalone*, document ETSI 3GPP TS 38.101-2 V15.3.0 Release 15, Oct. 2018.

[43] D. J. Griffiths, *Introduction to Electrodynamics*, 4th ed. Cambridge, U.K.: Cambridge Univ. Press, 2017.

[44] T. Tuovinen, K. Y. Yazdandoost, and J. Iinatti, "Comparison of the performance of the two different UWB antennas for the use in WBAN on-body communication," in *Proc. 6th Eur. Conf. Antennas Propag. (EUCAP)*, Prague, Czech Republic, Mar. 2012, pp. 2271–3374.

[45] *Proto Electronics, PCB FR4*. Accessed: Jun. 2020. [Online]. Available: https://www.proto-electronics.com/blog/the-4-electronic-component-suppliers-of-proto-electronics-0

[46] *Taconic TRF-43: The Guide to FR-4 for Your Printed Circuits*. Accessed: Jun. 2020. [Online]. Available: https://www.4taconic.com/page/trf-43-76.html

[47] M. Särestöniemi, V. Niemelä, M. Hämäläinen, J. Iinatti, N. Keränen, T. Jämsä, J. Partala, T. Seppänen, and J. Reponen, "Receiver performance evaluation on IEEE 802.15.6 based WBAN for monitoring Parkinson's disease," in *Proc. 8th Int. Symp. Med. Inf. Commun. Technol.*, Florence, Italy, Apr. 2014, pp. 1–5.

[48] M. Särestöniemi, C. Pomalaza-Ráez, T. Kumpuniemi, M. Hämäläinen, R. Kovacs, and J. Iinatti, "Measurement data-based study on the intrabody propagation in the presence of the sternotomy wires and aortic valve implant," *IEEE Trans. Antennas Propag.*, vol. 67, no. 8, pp. 4989–5001, Aug. 2019.
[49] *CST Microwave Studio*. Accessed: Jun. 2020. [Online]. Available: http://www.cst.com
[50] *CST Microwave Studio-Biological Data*. Accessed: Jun. 2020. [Online]. Available: http://www.mweda.com/cst/cst2013/mergedProjects/CST_EM_STUDIO/common_tools/bio_models.htm#Voxel_Family
[51] K. Turbic, L. M. Correia, and M. Beko, "A mobility model for wearable antennas on dynamic users," *IEEE Access*, vol. 6, pp. 63635–63648, Dec. 2018.
[52] J. D. Parsons, *The Mobile Radio Propagation Channel*, 2nd ed. London, U.K.: Wiley, 2000.
[53] G. Koutitas, "Multiple human effects in body area networks," *IEEE Antennas Wireless Propag. Lett.*, vol. 9, pp. 938–941, Sep. 2010.
[54] T. Alves, B. Poussot, and J.-M. Laheurte, "Analytical propagation modeling of BAN channels based on the creeping-wave theory," *IEEE Trans. Antennas Propag.*, vol. 59, no. 4, pp. 1269–1274, Apr. 2011.

KENAN TURBIC (Member, IEEE) was born in Sarajevo, Bosnia and Herzegovina, in 1988. He received the M.Sc. degree from the University of Sarajevo, in 2011, and the Ph.D. degree (Hons.) in electrical and computer engineering from IST, University of Lisbon, in 2019. He is currently a Postdoctoral Researcher with the INESC-ID Research Institute, Lisbon, Portugal. His main research interest includes wireless channel modeling, with a particular interest in body area networks. He has been actively participating in the COST Action CA15104 (IRACON), to which he has contributed with several technical documents and served as one of the Section Editors for the final report book.

MARIELLA SÄRESTÖNIEMI (Member, IEEE) received the M.Sc., Lic.Tech., and Dr.Tech. degrees from the University of Oulu, Finland, in 2003, 2005, and 2020, respectively. She is currently a Postdoctoral Researcher with the Centre for Wireless Communications, University of Oulu. Her research interests include medical ICT, wireless body area networks, in-, on-, and off-body propagation and communications, and simulation and measurement-based channel modeling.

MATTI HÄMÄLÄINEN (Senior Member, IEEE) received the M.Sc. and Dr.Sc. degrees from the University of Oulu, Finland, in 1994 and 2006, respectively. From 2016 to 2018, he was nominated as a Visiting Professor with the Institute of Advanced Science, Yokohama National University, Japan. He currently works as a University Researcher and an Adjunct Professor with the Centre for Wireless Communications, University of Oulu. He holds one patent. According to Google Scholar, his current H-index is 26. His research interests include radio channel modeling, UWB systems, wireless body area networks, and medical ICT. He is a Fellow of the EAI Community. He is a member of the External Advisory Board of the WiMed Research Centre, Macquarie University, Australia, and the Editorial Board of *Annals of Telecommunications*. He is also an Active Member at ETSI TC SmartBAN. He is the Co-Chair of the International Steering Committee of ISMICT Conference. He is also an Associate Editor of IEEE Access and *Frontiers in Communications and Networks*—the Non-Conventional Communications and Networking Section.

LUIS M. CORREIA (Senior Member, IEEE) was born in Portugal, in 1958. He received the Ph.D. degree in electrical and computer engineering from IST, University of Lisbon, in 1991. He is currently a Professor in telecommunications with IST, University of Lisbon, with his work focused on wireless and mobile communications in the areas of propagation, channel characterization, radio networks, traffic, and applications, with the research activities developed at the INESC-ID Institute. He has acted as a Consultant for the Portuguese telecommunications operators and regulator, besides other public and private entities, and he has been in the Board of Directors of a telecommunications company. Besides being responsible for research projects at the national level, he has participated in 31 projects within European frameworks, having coordinated six and taken leadership responsibilities at various levels in many others. He has supervised more than 200 M.Sc./Ph.D. students, having edited six books, contributed to European strategic documents, and authored more than 500 articles in international and national journals and conferences, for which he also served as a reviewer, an Editor, and a Board Member. Internationally, he was a part of 36 Ph.D. juries, and 66 research projects and institutions evaluation committees for funding agencies in 12 countries, and the European COST and Commission. He has been the Chairman of the Technical Programme Committee and the Steering Committee of various major conferences, besides other several duties. He was the National Delegate of the COST Domain Committee on ICT. He was active in the European Networks Platform, by being an Elected Member of the Expert Advisory Group and the Steering Board, and the Chairman of the Working Group on Applications. He was also elected to the European 5G PPP Association. He has launched and served as the Chairman of the IEEE Communications Society Portugal Chapter.